CEAS Aeronautical Journal (2021) 12:307–329
https://doi.org/10.1007/s13272-021-00492-z

ORIGINAL PAPER

# Rotorcraft fuselage mass assessment in early design stages

**Dominik B. Schwinn[1] · Peter Weiand[2] · Michel Buchwald[2]**

Received: 14 August 2020 / Revised: 21 December 2020 / Accepted: 20 January 2021 / Published online: 25 March 2021


**Abstract**
Like the design of fixed-wing aircraft the design of rotorcraft is generally divided into the three consecutive phases of conceptual, preliminary and detailed design. During each phase the acquired results in turn serve as input for new calculations, thus increasing the detail level and information about the new concept, while uncertainties about the new design are reduced. An important aspect of the overall design process is the mass estimation in early design stages. The weight of the rotorcraft drives the design of many important components, such as the rotor(s), the propulsion system and, therefore, the required fuel. The fuselage is considered as the central structural part, since it connects all other components to each other and serves as protection of the occupants but in the past it often turned out to also be the heaviest part of all rotorcraft components. This paper shows an approach to estimate rotorcraft component masses using statistical methods based on existing rotorcraft but also an approach to use finite element methods that determine the structural airframe mass based on mission profiles, respectively, bearable load cases.

**Keywords** Rotorcraft design · Mass estimation · Structural Analysis · Conceptual and preliminary design · Fuselage sizing

**List of symbols**

| | |
|---|---|
| $f$ | Surface correction factor |
| $f_{\text{ramp}}$ | Factor to consider cargo ramp installation |
| $h$ | Height |
| $L$ | Tool level |
| $l$ | Length |
| $m_{\text{comp}}$ | Component mass |
| $l_{\text{fus}}$ | Fuselage length |
| $m_{\text{em}}$ | (basic) Empty mass |
| $m_{\text{fe}}$ | Furnishings and equipment group mass |
| $m_{\text{fuel}}$ | Fuel mass |
| $m_{\text{fus}}$ | Fuselage mass |
| $m_{\text{mto}}$ | Maximum take-off mass |
| $m_{\text{oem}}$ | Operating empty mass |
| $m_{\text{oi}}$ | Operator items mass |
| $m_{\text{pay}}$ | Payload |
| $m_{\text{prop}}$ | Propulsion group mass |
| $m_{\text{struct}}$ | Structural group mass |
| $m_{\text{sys}}$ | Systems group mass |
| $n_i$ | Number of interfaces |
| $n_t$ | Number of design tools |
| $n_z$ | Design ultimate load factor |
| $R_c$ | Ratio of actual versus critical compressive stress |
| $R_s$ | Ratio of actual versus critical shear stress |
| $s_b$ | Body surface |
| Si | Stringer section number $i$ |
| $\text{SF}_{\text{str}}$ | Safety factor for strength |
| $\text{SF}_{\text{stab}}$ | Safety factor for stability |
| $t$ | Thickness |
| $w$ | Width |
| $W_e$ | Empty weight (in lb, corresponds to $m_{\text{em}}$) |
| $W_g$ | Design gross weight (in lb, corresponds to $m_{\text{mto}}$) |
| $\sigma_c$ | Compressive stress |
| $\sigma_{c,\text{crit}}$ | Critical compressive stress |
| $\sigma_{\text{eqv}}$ | Equivalent stress |
| $\sigma_{\text{eqv,max},a}$ | Maximum allowable equivalent stress |
| $\tau$ | Shear stress |
| $\tau_{\text{crit}}$ | Critical shear stress |
| $\chi_{\text{fus}}$ | Fuselage technology factor |
| $\chi_i$ | Technology factor for component $i$ |

**Abbreviations**

| | |
|---|---|
| AFDD | U.S. Army Aeroflightdynamics Directorate |
| APDL | ANSYS Parametric Design Language |
| COG | Center Of Gravity |

✉ Dominik B. Schwinn
dominik.schwinn@dlr.de

[1] German Aerospace Center (DLR), Institute of Structures and Design, 70569 Stuttgart, Germany

[2] German Aerospace Center (DLR), Institute of Flight Systems, 38108 Braunschweig, Germany

| | |
|---|---|
| CPACS | Common Parametric Aircraft Configuration Schema |
| DFEM | Detailed FEM |
| DLR | German Aerospace Center (Deutsches Zentrum für Luft- und Raumfahrt) |
| EDEN | Evaluation and Design of Novel Rotorcraft Concepts |
| FE | Finite Elements |
| FEM | Finite Element Method |
| FSD | Fully Stressed Design |
| GFEM | Global FEM |
| HOST | Helicopter Overall Simulation Tool |
| IRIS | Integrated Rotorcraft Initial Sizing |
| PANDORA | Parametric Numerical Design and Optimization Routines for Aircraft |
| RCE | Remote Component Environment |
| RIDE | Rotorcraft Integrated Design and Evaluation |
| SAWE | Society of Allied Weight Engineers |
| TIGL | TIVA Geometric Library |
| TIVA | Technology Integration for the Virtual Aircraft |
| TIXI | TIVA XML Interface |
| TLAR | Top Level Aircraft Requirement |
| TRIAD | Technologies in Integrated and Advanced Design |
| UTH | Utility/Transport Helicopter |
| XML | Extensive Markup Language |

## 1 Introduction

Designing a new rotorcraft is a complex challenge. Like fixed-wing aircraft it involves different disciplines. To get the optimum design, the multiple disciplines have to interact right from the start.

In general, aircraft design is separated into three classical stages, for instance as given by [1]: the conceptual phase, the preliminary phase, and the detailed design phase.

The conceptual design is mainly driven by the attempt to determine the external configuration that fulfills the Top Level Aircraft Requirements (TLARs). Typical (and frequently used) TLARs are for instance range, payload, cruise speed, or cabin volume. The generation of a concept study already involves several disciplines. To assess different concepts the design engineers need fast analysis methods due to the size of the design space and time and resource limits that constraint its exploration. Therefore, the tools used in the conceptual design phase feature many simplifications. Generally, the conceptual design stage can be considered as finished when the major design parameters have been established, such as the generation of an outer aerodynamic surface, often referred to as loft (exemplary see Fig. 1).

The preliminary design uses higher fidelity tools to account for an increasing detail level. In this design stage a basic internal arrangement is elaborated. Structurally seen, the aforementioned outer configuration is provided with primary structure, such as frames, stringers, and fuselage skin panels. The distribution of the primary structure follows knowledge based engineering rules. Typical requirements are the reinforcement of fuselage cutouts to bypass the loads around openings, such as doors. Other requirements arise due to the positioning of the main rotor which requires a reinforced mounting to the airframe. The possible design solutions in this phase follow a much narrower path than in the conceptual design phase. Due to the information gained in the conceptual design stage there is more input available for the calculations but there is also both more and more detailed output, so that the tools in this design phase often require more computational power and processing times.

The detailed design phase deals with detailed solutions, often driven by manufacturability reasons. The tools used in this stage feature the highest demand of computational resources, labor time, and manpower.

A fundamental part of the design process is the mass estimation. In the conceptual design stage the mass estimation is required to define and assess the required flight performance of the novel rotorcraft. In the preliminary design stage the ground and flight loads, which result from the estimated mass, are the basis for the structural sizing which in turn influences the weight and, therefore, the flight performance. In this phase the term *mass estimation* turns into the term *mass assessment*, since the results are not purely based on statistics anymore, therefore, the deviation from the true weight is expected to decrease. In the detailed design phase the mass estimation can be considered as a constraint, since any additional weight penalties, caused by constructional requirements, may negatively influence the mass and thus, the desired flight performance. It shall be noted at this point that the flight performance is affected by the rotorcraft weight at all time. Therefore, the rotorcraft weight must be tracked carefully during the complete design process.

**Fig. 1** Implemented rotorcraft configurations

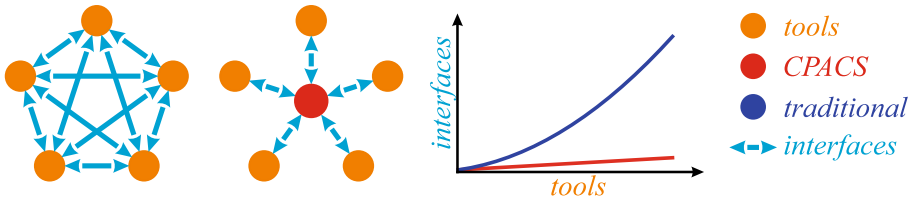


**Fig. 2** CPACS benefits

The fuselage represents an important part of the rotorcraft. It serves as a central mounting for major components (e.g., rotors, gear box, alighting gear, aerodynamic control surfaces) and also as an aerodynamic shielding for the occupants accommodated in the cabin within. Consequently it often represents the heaviest component of the overall rotorcraft. Therefore, the fuselage features high weight saving potential and deserves a more detailed examination.

In 2010, the German Aerospace Center (DLR) started with the generation of an automated and integrated design environment for rotorcraft. To assess novel rotorcraft configurations addressing typical rotorcraft limitations, such as speed or noise. During the projects Rotorcraft Integrated Design and Evaluation (RIDE, [2]) and Evaluation and Design of Novel Rotorcraft Concepts (EDEN, [3, 4]) the data model Common Parametric Aircraft Configuration Schema (CPACS, [5]) was adapted to match parametric rotorcraft description. The network based simulation environment Remote Component Environment (RCE, [6]) was used to set up the workflows for the design processes of generic rotorcraft. Within the DLR internal project Technologies for Rotorcraft in Integrated and Advanced Design (TRIAD, [7]), which started in 2018, the tools developed in the preceding projects were integrated into the new design environment Integrated Rotorcraft Initial Sizing (IRIS) to evaluate and assess new virtual rotorcraft configurations (e.g., high-speed rotorcraft). The tools used in this environment cover the phases of conceptual, and partly the preliminary design.

This paper describes the mass estimation processes in the conceptual design stage established within the aforementioned projects. Moreover, it shows an approach to assess the fuselage mass in the preliminary design stage.

## 2 Design environment

One of the primary features of this design environment is the use of a distributed computation. Therefore, IRIS constitutes a combination of RCE as collaboration software connecting the different servers, and the CPACS data model as a universal language between the individual tools.

Starting a highly iterative design process requires the setup of an initial configuration at the beginning. The minimum required TLARs are most commonly payload, range, maximum cruise speed and the rotorcraft configuration (standard configuration with main and tail rotor, coaxial configuration, and tandem configuration) as shown in Fig. 1. These parameters are specified by the customer, respectively, the user at the beginning of the design study. In the presented process the number of rotor blades is a value that has to be specified by the user in advance to the sizing process. Other parameters are calculated by either statistical or physical methods during the design process.

A major aspect to handle an integrated and automated tool chain is a seam- and flawless connection and communication between all involved tools. As language to describe the rotorcraft and to control the input and output of the tools, the in-house developed CPACS data model was chosen and extended by the specific data describing rotorcraft. The additional data basically consist of the description of the rotors, which is typically not covered by fixed-wing design.

The CPACS data model serves as interface between the involved tools. In the beginning of the design process, it is an empty file that is filled with results after each analysis, thus increasing the detail level. Certain tools require input that must be computed by other tools first, therefore, the tool order must be arranged wisely.

CPACS is an XML based data model to describe parametric aircraft. Its benefits are its hierarchical structure, readability, and easy access. Using CPACS as integral key component for data exchange, the amount of required tool interfaces can be significantly reduced, thus increasing clarity of the calculation modules. The quantity of required tool interfaces is reduced from a quadratic approach for the traditional design approach

$$n_i = n_t\left(n_t - 1\right), \tag{1}$$

to a linear approach

$$n_i = 2n_t, \tag{2}$$

with CPACS as common design language.

Figure 2 shows an interface scheme of the traditional approach, where each tool directly communicates with any other tool (on the left) and the alternative approach (middle), enabled by the use of CPACS as centralized data storage, while the graph on the right schematically visualizes the reduction of interfaces indicating simplified maintenance.

Other advantages of CPACS are that the data model of the input and output files is identical, i.e., individual tools can

easily be replaced and workflows can be rearranged without intensive reprogramming.

To efficiently work with the CPACS data model the two libraries TIXI (TIVA[1] XML Interface, [9]) and TIGL (TIVA Geometric Library, [10]) are used, since they provide standardized routines to access the data within CPACS. TIXI is a library for the handling of input and output data in text format, while TIGL is a graphic library that provides functions to process geometric information of the aircraft model.

To set up workflows that connect and execute the tools developed by the participating institutes the in-house software RCE was chosen: Each institution provides a server with its tools locally installed. A CPACS file is then sent from tool to tool (and thus from server to server) using an internal network. Each computation fills, respectively, updates the CPACS file with more and more detailed data. Therefore, the CPACS file serves as input but also as output for all computations. The advantages of RCE are that tools never leave the institution, where they were developed, i.e., the source code (and, therefore, the disciplinary knowledge) always remains at the facility, where it was designed. Moreover, maintenance, development, and testing of the tools is eased as they stay on-site allowing an easy access for the responsible engineers.

With respect to the computation time, the uncertainties, the robustness, and the amount of required input data the variety of design tools applies to different methods of modeling. Hence they are classified into four major fidelity categories ranging from level L0 to L3:

- L0 tools: They mostly use empirical methods with many very simple physical assumptions. They provide much output with only very limited input. A typical application is the initial sizing as depicted in Fig. 3.
- L1 tools have a better physical modeling but still are fast enough to perform iterative procedures. Therefore, they are widely used for primary sizing tasks, (see Fig. 4). This class of tools is used for the conceptual design part in IRIS.
- L2 tools feature a very good physical modeling. As a disadvantage, they require much computational power and a more detailed input to work reliable. They produce a high amount of output which cannot always be handled automatically.
- L3 tools are considered as the most complex design tools. They have the highest computational demand with regard to power and time. Moreover, their pre-processing of the computational model and the post-processing of the calculated results cannot be performed automatically. This class of tools is typically used during the detailed design phase.

[1] TIVA (Technology Integration for the Virtual Aircraft) was a DLR project from 2005 to 2009 that marks the beginning of extensive multidisciplinary collaborations at DLR [8].

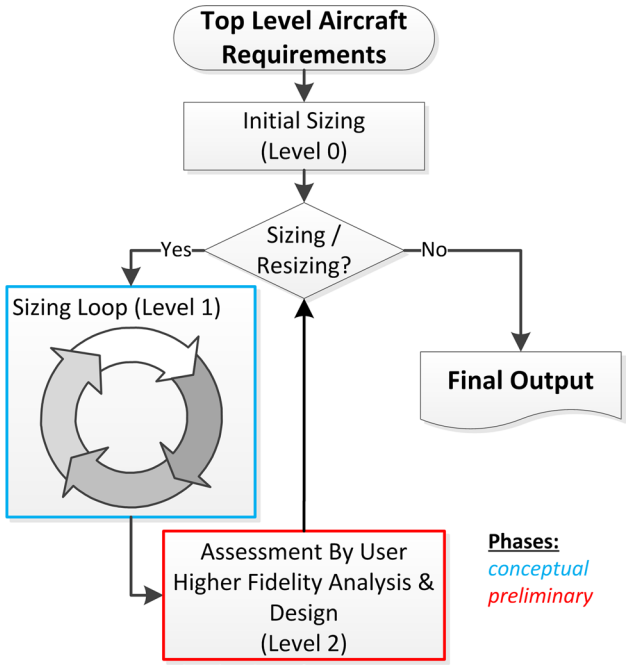


**Fig. 3** Flowchart of the virtual design approach [11]

The general process structure, as it is currently implemented in IRIS, is schematically illustrated in Fig. 3.

In general, an initial sizing is conducted using L0 tools to create a first data set. The L1 tools complete the data and the L2 tools extend the data.

The TLARs dictate a primary configuration with an initially estimated design gross weight which corresponds to the maximum take-off mass $m_{\mathrm{mto}}$. At this early stage of the design process it is roughly estimated by L0 tools using statistical methods. This approach impedes novel design approaches, since statistical data is not sufficiently available.

The sizing loop (depicted in blue) is conducted using L1 tools and corresponds to the conceptual design phase. The arrangement of the L1 tools of the sizing loop from Fig. 3 is illustrated as flowchart in more detail in Fig. 4. If $m_{\mathrm{mto}}$ has converged during this stage, the design process shifts to the preliminary design phase (corresponds to the red box in Fig. 3).

Higher fidelity tools are used to further optimize the configuration of the conceptual design stage during the preliminary design phase (red box in Fig. 3). Since the computation times of L2 tools usually exceed the demanded limits of the conceptual design stage, they are used outside the sizing loop. If the results of the higher fidelity computations show major deviations between the L1 and L2 tools, technology

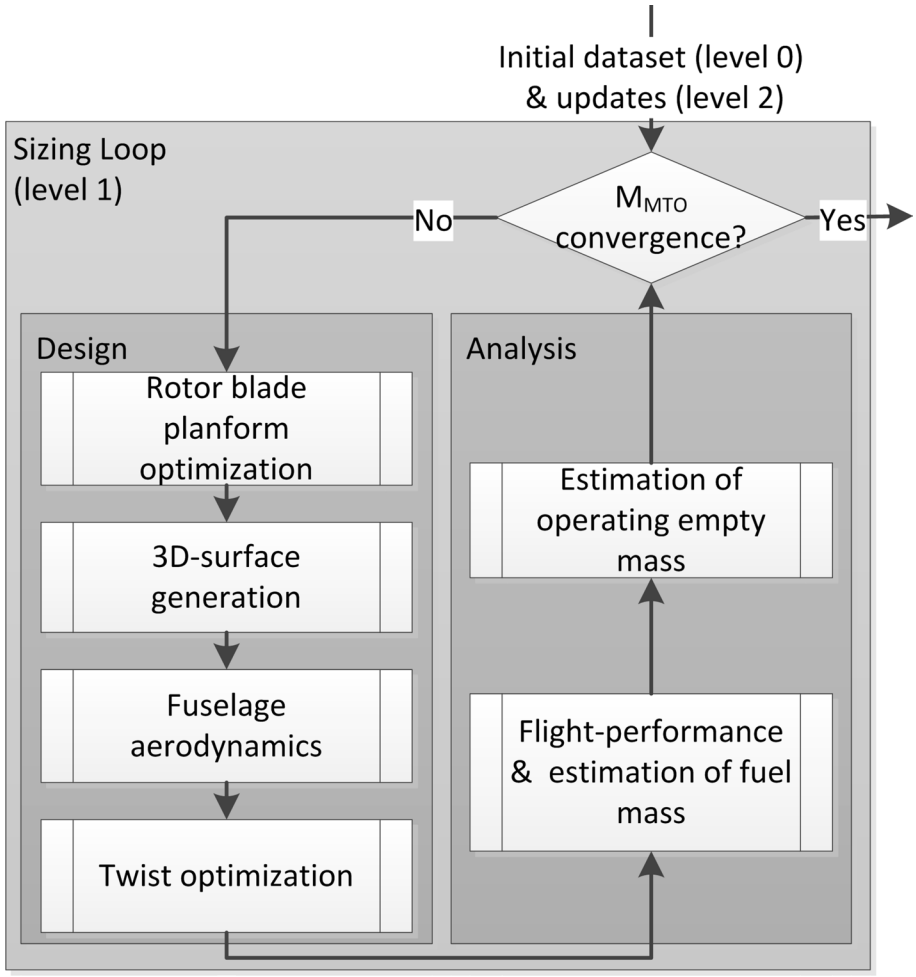


**Fig. 4** Flowchart of the L1 sizing loop

factors may be recalibrated to perform a resizing of the configuration with the L1 tools, because these deviations may result in major deviations in the maximum take-off mass influencing, e.g., rotor dimensions, flight performance, fuel consumption.

Figure 4 shows the sizing loop of Fig. 3 in detail. Depending if the input is from the initial dataset (with L0 tools) or from a resizing (after L2 tools have been applied), the input for this sizing loop may vary.

In the initialization phase, an empty CPACS file is generated and a basis configuration is stored. Based on a dataset of about 160 helicopters, a first maximum take-off mass is estimated, serving as starting point for the subsequent sizing processes.

During the design branch of the sizing loop, the design of the configuration is developed to account for the TLARs, respectively, requirements that have been generated by previous tools. The primary and most important step in the sizing loop is the calculation of the main rotor dimensions, as its characteristics are substantial for the performance of the overall design. A knowledge based procedure [12] is applied for the optimization of the rotor radius, blade chord length, and blade tip speed using aspect ratio, blade loading, advance ratio, energy ratio and the Lock number as optimization constraints.

After the sizing of the rotors, a three dimensional model of the rotorcraft is developed by sizing a generic fuselage assembly with respect to the determined component scales. The responsible tool automatically instantiates fuselage components from a catalogue and scales them to match the required overall dimensions. The geometry model is automatically generated in CATIA and subsequently transformed into the CPACS denoted description of profiles and sections for further geometric processing, e.g., aerodynamic or structural analyses. Figure 5 shows how the fuselage is assembled by the individual components. A detailed description of the geometry generation module is given by Kunze [13].

Figure 6 shows the different fuselage types that are created and stored in the CPACS file. The inner fuselage represents the cabin for the crew, passengers and cargo. The structural fuselage represents the fuselage that carries the structural loads. The aerodynamic fuselage often coincides

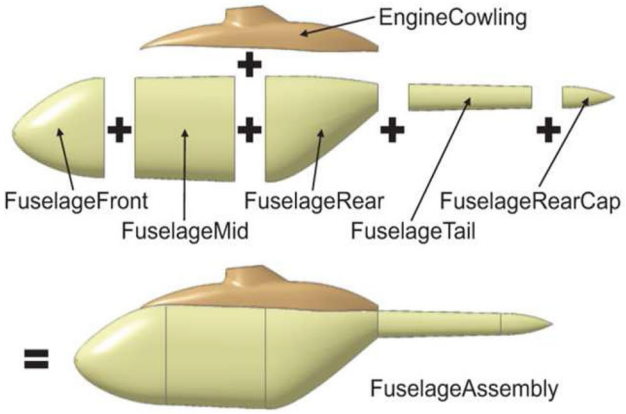


**Fig. 5** Assembly of fuselage components

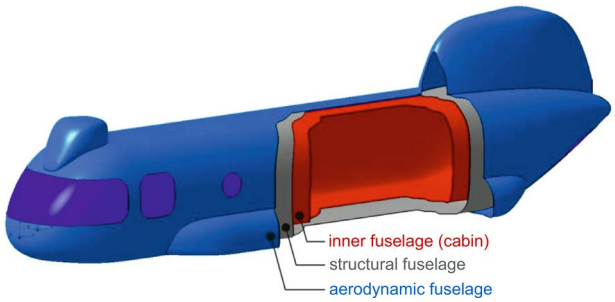


**Fig. 6** Different fuselage types in CPACS

with the structural one. However, certain components that do no not carry load but serve as aerodynamic cowling (e.g., the fuel tank fuselage side fairing in Fig. 6) induce differences to the structural fuselage. It shall be noted at this point that the structural analysis and sizing processes, as introduced in Sect. 5, refer to the structural fuselage.

Subsequently, the aerodynamic properties of the clean fuselage are calculated by a module which is based on the commercial tool VSAERO [14]. Corrections that consider drag by landing gears, rotor hub(s), and other attachments are applied to the results of the clean fuselage by the use of handbook methods [15, 16], while the polars of the stabilizers are calculated separately.

An iterative optimization of the blade twist is performed minimizing the required power for the design flight condition (in this case cruise speed). The trim calculation for this procedure is conducted using the tool HOST (Helicopter Overall Simulation Tool, [17]). In this calculation the maximum collective pitch angle is the only constraint used to keep the controls in a reasonable range.

In the analysis branch of the sizing loop the maximum take-off mass is recalculated. With the flight performance calculation the required fuel mass for the design mission is computed iteratively using HOST: For all flight segments, trim calculations are performed at the beginning and at the end of every segment to obtain the required power to predict the mean fuel flow and actual range. The actual and required range are compared to each other which leads to a correction of the actual fuel mass until it converges and the required range is met. A more detailed description of the flight performance analysis and the estimation of the fuel mass is given by Buchwald et al. [18], while Weiand et al. [11, 19] provide more information on the overall design process.

The component mass estimation concludes the analysis section of the sizing loop as enough parameters have been calculated to create a mass breakdown allowing for a more precise $m_{\mathrm{mto}}$. This updated maximum take-off mass then serves as input for sizing loop iterations. Convergence of $m_{\mathrm{mto}}$ marks the end of the conceptual design phase so that the external configuration with the derived mass breakdown and the corresponding required flight performance are available in a reasonable and consistent relation for further evaluation in the preliminary design stage.

The mass estimation process in general is described in more detail in Sect. 3, while the statistical approaches for the conceptual design phase implemented in IRIS are introduced in Sect. 4.

## 3 Mass estimation

Mass estimation is a fundamental part of the overall design process. The design gross weight is considered as a central design parameter. It determines and influences many design parameters. As example, the maximum take-off mass $m_{\mathrm{mto}}$ of the helicopter determines the rotor characteristics, since the rotor has to generate the necessary lift for hovering and flight. The power to drive the rotor, in turn, dictates the engine(s) which then determines the fuel amount to successfully conduct the requested missions. These components in turn influence other component masses, such as gear box, drive system, hydraulics, electrics, etc. as well as the structural mass. The reduction of fuel mass and thus $m_{\mathrm{mto}}$ is a major objective in aeronautical design as it has a favorable effect on flight performance and operating expenses [20]. Estimating $m_{\mathrm{mto}}$ too low may lead to a comparable weak structure which might deform irreversibly (or even fail) under extreme conditions (i.e., if the designers estimate the weight too low, they will design a lighter structure, e.g., smaller and/or thinner structural elements, smaller engines, etc., because they assume that the rotorcraft will not be that heavy. But if the actual weight during detailed design or manufacturing becomes heavier than what they assumed, there will arise the problems of insufficient performance or structural safety. These circumstances may lead to structural failure, because the loads, caused by inertia of the masses

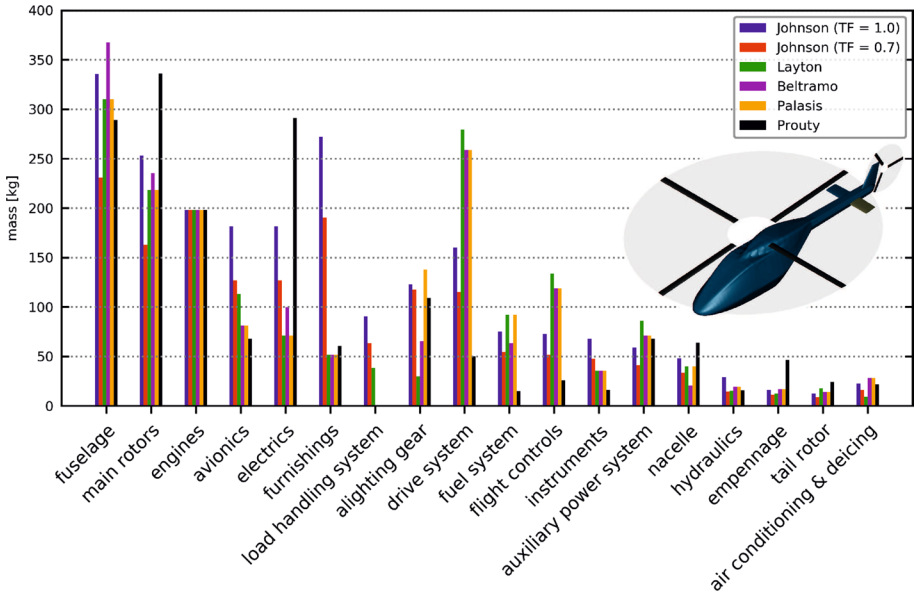


**Fig. 7** Comparison of the implemented mass estimation methods

that are higher than what the rotorcraft was designed to withstand, will not be bearable). In contrast, estimating $m_{\mathrm{mto}}$ too high may lead to an excessive structural weight which reduces the efficiency and increases cost, because the rotorcraft has to carry dead weight during each flight. Therefore, an estimation of $m_{\mathrm{mto}}$ as precise and early as possible is an important and essential task during the design process. The maximum take-off mass $m_{\mathrm{mto}}$ is of particular interest in the design process, since it represents the heaviest configuration of an aircraft at which it has to fulfill all applied airworthiness requirements. It can be broken down into

$$m_{\mathrm{mto}} = m_{\mathrm{oem}} + m_{\mathrm{pay}} + m_{\mathrm{fuel}}. \tag{3}$$

In general, the payload is a requirement specified by the customer and consists of passengers and/or cargo. The operating empty mass $m_{\mathrm{oem}}$ represents the empty aircraft ready to be operated. It is broken down into

$$m_{\mathrm{oem}} = m_{\mathrm{oi}} + m_{\mathrm{em}}, \tag{4}$$

with $m_{\mathrm{em}}$ representing the dry, empty mass of the rotorcraft. The so-called operator items mass $m_{\mathrm{oi}}$ represents the mass of items which are added to operate the rotorcraft as intended. Examples for $m_{\mathrm{oi}}$ are seats (required for the crew, optional for passengers), safety equipment, system fluids but also cabin amenities such as entertainment systems. It shall be noted that the crew mass $m_{\mathrm{crew}}$ itself has been integrated into $m_{\mathrm{oi}}$ in the presented processes. The dry, empty mass $m_{\mathrm{em}}$ is calculated as sum of the aircraft group masses

$$m_{\mathrm{em}} = m_{\mathrm{struct}} + m_{\mathrm{prop}} + m_{\mathrm{sys}} + m_{\mathrm{fe}}. \tag{5}$$

The group masses represent the sum of the individual contained components. The component mass estimation within IRIS follows the standards proposed in Recommended Practice Number 8 (RP 8) [21] by the Society of Weight Engineers (SAWE).

## 4 Statistical mass estimation

In the early conceptual design only limited data is available. Therefore, at that time of the design process, statistical approaches are used to estimate the rotorcraft mass breakdown. However, novel configurations can only be roughly estimated by comparison to already existing rotorcraft of similar configuration. In the presented design environment IRIS the methods proposed by Beltramo and Morris [22], Layton [23], Palasis [24], Prouty [25], and the AFDD (U.S. Army Aeroflightdynamics Directorate) models provided by Johnson [26] have been implemented. Figure 7 shows a comparison of the different mass estimation methods for a generic medium-sized utility rotorcraft in standard configuration with a comparable mission profile to the reference configuration, a highly modified EC135 [27].

It can be observed that the methods provided by Johnson seem to estimate the highest masses when a calibration of the models by technology factors is not conducted. Technology factors can be applied for each component (and its $j$ subcomponents) to individually scale the estimated component mass according to

$$m_{\mathrm{comp}} = \sum_{j=1}^{n} \chi_j m_j. \tag{6}$$

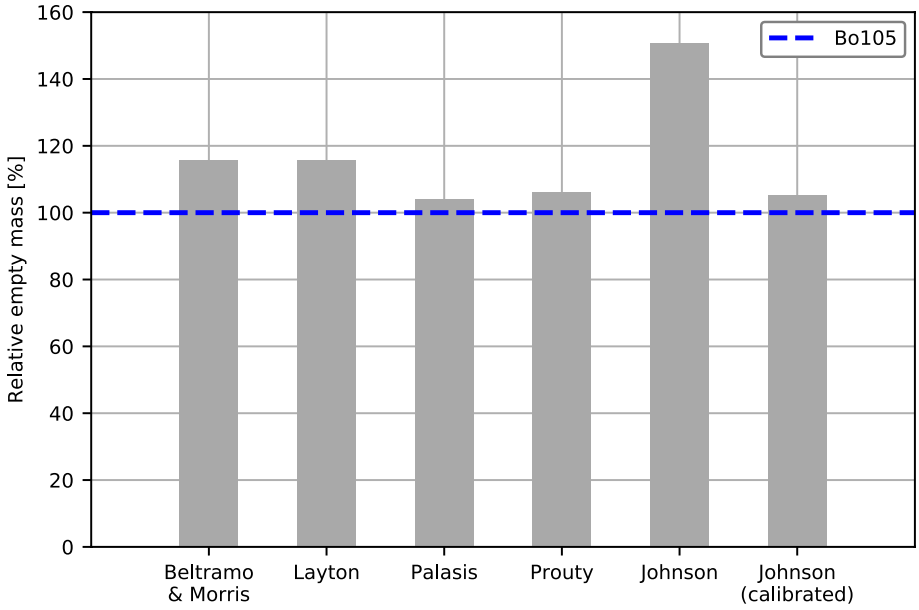


**Fig. 8** Comparison of the implemented mass estimation methods for a Bo105

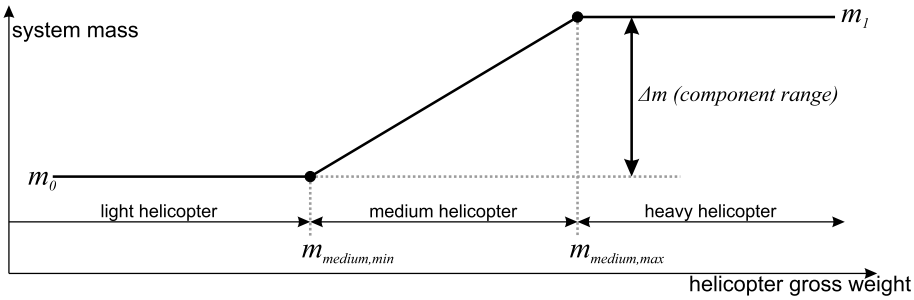


**Fig. 9** Linear interpolation of system masses

As an example, the fuselage component consists of additional elements to account for crashworthiness, alighting gear integration, tail and/or wing folding mechanisms, marinization, pressurization, etc.

The estimation of the correct technology factor for each individual component is a challenge which, in general, requires sophisticated knowledge about the mass breakdown of a reference configuration. Since this type of information is very sensitive to the manufacturers, it is rarely published, and therefore, this circumstance complicates the estimation of the correct technology factors. Because the reference configuration is in continuous operational use, a complete demounting for individual calibration of each technology factor was impossible. However, as the maximum take-off mass of the reference configuration, including the shares of payload mass, basic empty mass, and fuel mass is known [19], it was reasonable to apply one common technology factor to all component masses. The use of an overall technology factor for all components smears the component masses for the sake of a correct estimation of $m_{\mathrm{mto}}$. This approach was also performed by Russel and Basset [28]. A technology factor of $\chi = 0.7$ led to a deviation of about 3% of the estimated $m_{\mathrm{mto}}$ to the reference configuration $m_{\mathrm{mto,ref}}$. Applying this technology factor to a Bo105, which is a similar configuration of the same weight class, good agreement could be observed for $m_{\mathrm{em}}$ (shown in Fig. 8), thus confirming the chosen technology factor.

It shall be stated that the use of one common technology factor is seen debatable as deviations for certain components might cancel each other. In this case, $m_{\mathrm{mto}}$ may still be correct but different component masses will eventually lead to different results for the structural analysis. However, as long as no detailed component masses are available for validation purposes, the use of a common technology factor is considered as a justifiable approach for an early mass estimation.

The mass estimation of some systems in IRIS follows an approach based on Johnson's methods: Certain systems, such as, e.g., instruments or hydraulics, are estimated by linear interpolation between lower and upper limits for medium to heavy weight helicopters, as illustrated in Fig. 9. Alternatively, fixed masses for these systems can be specified. In case, a certain component mass is known (or desired) it can be stored in the corresponding CPACS node and will not be changed in subsequent iterations.

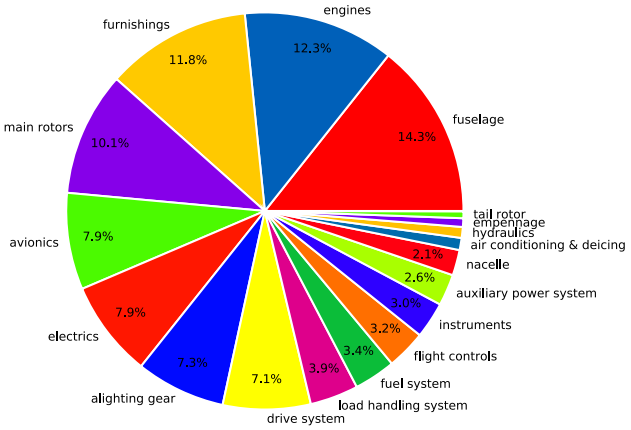


**Fig. 10** Composition of $m_{\text{em}}$ (calibrated AFDD models)

A composition of the empty mass calculated using the calibrated AFDD models (as displayed in Fig. 7) is shown in Fig. 10. It is observable that the fuselage mass constitutes the highest share. It shall be noted that this composition represents one specific, generic configuration. However, the shares of the individual components can be considered as comparably precise and, therefore, representative for any given rotorcraft configuration. Thus, the fuselage can be considered as a major design driver concerning weight, offering high weight saving potential.

Comparing the aforementioned methods to estimate rotorcraft component masses it can be observed that the body surface $s_b$ constitutes an important parameter for the estimation of certain components. Beltramo and Morris use one regression formula for the fuselage mass $m_{\text{fus}}$ which is a function merely of the body surface $s_b$:

$$m_{\text{fus}} = f(s_b). \tag{7}$$

They do not differentiate between different weight classes or rotorcraft types. Like Beltramo and Morris, Layton's fuselage mass estimation depends solely on the body surface. However, Layton classifies three different weight types of helicopter (see Table 1) and provides a formula for each.

The approach of Palasis in general can be seen as a mixture of the formulas provided by Beltramo and Layton, and therefore, it will not be described in detail within this paper. The earlier methods, represented by Beltramo and Morris, and Layton that solely depend on the body surface are shown in Fig. 11. As mentioned earlier, Layton groups rotorcraft in three different weight classes depending on their $m_{\text{mto}}$: It can be observed from Fig. 11 that, for instance, the use of his *light rotorcraft*—formula would lead to an excessive estimation of the fuselage mass for a heavier weight class with increasing body surface. Note, that the formula for heavy helicopters has not been included in the diagram due to clarity reasons, since it is not applicable in the presented body surface range.

**Table 1** Weight classes according to Layton

| Weight class | $m_{\text{mto}}$ range [lb] |
|---|---|
| Light | $m_{\text{mto}} < 3000$ ($\approx 1360.78$ kg) |
| Medium | $3000 \leq m_{\text{mto}} \leq 25,000$ ($\approx 11,339.81$ kg) |
| Heavy | $m_{\text{mto}} > 25,000$ |

As mentioned above, the body surface $s_b$ represents an important parameter for the mass estimation process, since it coarsely overviews the size, thus the overall weight of the rotorcraft. Within IRIS it can be calculated by two possibilities:

- TIGL functions, or
- Approximations provided by Layton.

The mass estimation module supports both methods. However, instabilities could be observed for the body surface calculation with TIGL functions. Therefore, the surface calculation follows the *try-except-rule*[2]: If the TIGL calculation fails, the approximation formulas by Layton are applied. These functions are provided for three different weight classes of helicopter:

$$s_{b,\text{light}} = 194.274 \cdot \ln(W_e) - 1306.779, \tag{8a}$$

$$s_{b,\text{medium}} = 636.081 \cdot e^{(0.0000098 \cdot W_g)}, \tag{8b}$$

$$s_{b,\text{heavy}} = 426.378 \cdot e^{(0.000045 \cdot W_g)}. \tag{8c}$$

Considering the fuselage mass estimations provided by Beltramo and Morris it is observable that for very small rotorcraft ($s_b < \approx 10$ m$^2$) the use of their method might lead to negative fuselage masses. This must be taken into account when being applied to very small rotorcraft representing urban mobility concepts, similar to, e.g., the Volocopter [29] or Ehang 184 [30] that are shown below in Figs. 12 and 13.

Taking the cockpit (respectively, fuselage) dimensions as specified by Volocopter [29] and Ehang [30], and assuming a cuboid shape which leads to a conservative body surface (i.e., the real body surface is less than assumed), results in the estimated fuselage masses as shown in Table 2.

[2] The try-and-except block in Python is used to handle exceptions. In case the code in the *try*-block fails, the code in the *except*-block is executed, thus avoiding an erroneous termination of the regular code caused by an error arising in the *try*-block. In case the *try*-block does not fail, the *except*-block will not be executed.

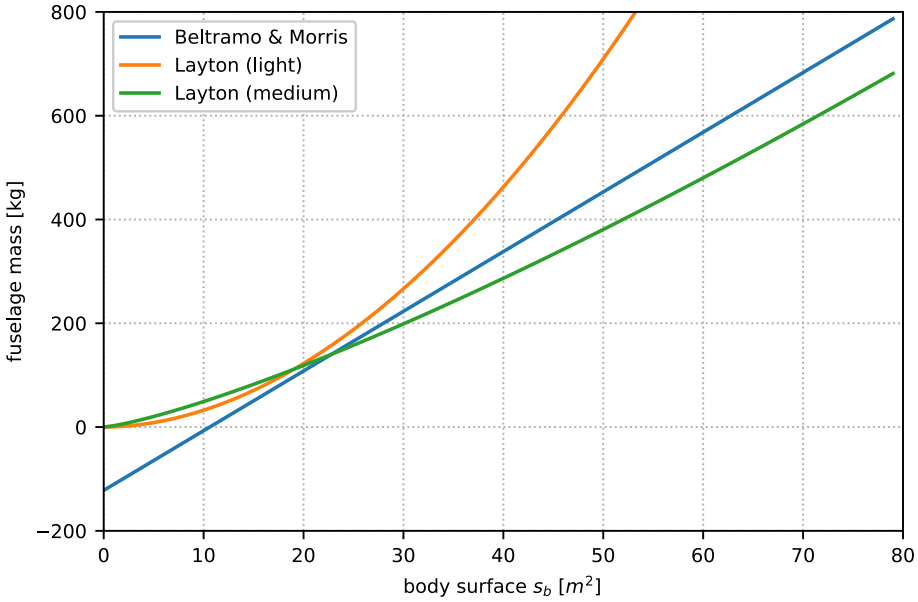


**Fig. 11** Fuselage mass calculation (Beltramo and Morris, and Layton) as function of body surface

**Fig. 12** Volocopter [29]

**Fig. 13** Ehang 184 [30]

**Table 2** Dimensions and estimated fuselage masses (Beltramo and Morris) for urban mobility concepts (values rounded)

| Rotorcraft | $l$ [m] | $w$ [m] | $h$ [m] | $s_b$ [m$^2$] | $m_{fus}$ [kg] |
|---|---|---|---|---|---|
| Volocopter | 3.20 | 1.25 | 1.21 | 18.77 | 93.87 |
| Volocopter ($f = 0.9$) | | | | 16.89 | 72.28 |
| Volocopter ($f = 0.8$) | | | | 15.02 | 50.69 |
| Ehang 184 | 2.07 | 1.02 | 1.45 | 13.17 | 29.5 |
| Ehang 184 ($f = 0.9$) | | | | 11.85 | 14.33 |
| Ehang 184 ($f = 0.8$) | | | | 10.54 | -0.82 |

Assuming surface correction factors of $f = 0.8$ and $f = 0.9$ to account for the deviation of the presumed cuboid shape to the real shape (for instance with regard to the inclined aerodynamic front resp. windshield), the fuselage mass can turn negative for the Ehang 184, highlighting the sensitivity of applying these methods to urban mobility concepts. Therefore, the aforementioned methods shall be applied with caution to prevent defective mass estimations for rotorcraft configurations other than the typical ones, as shown in Fig. 1.

It shall also be noted that, at the time Beltramo and, Morris and Layton published their methods, the use of composite materials was comparatively rare so that the presented methods are mainly based on metallic structures. A calibration of the methods with respect to composite material has not been performed yet. Constituting an enhancement for the mass estimation of rotorcraft fuselages, Prouty and Johnson reduced the dependence on the body surface by increasing the parameter range for the fuselage mass on additional factors, as shown in Eqs. 9 and 10:

$$m_{\text{fus}} = f(m_{\text{mto}}, l_{\text{fus}}, s_b). \tag{9}$$

Like Beltramo and Morris, Prouty and Johnson only provide one general method for the fuselage mass estimation for all rotorcraft weight classes. The AFDD model 82, as provided by Johnson, introduces additional dependencies:

$$m_{\text{fus}} = f(\chi_{\text{fus}}, f_{\text{ramp}}, m_{\text{mto}}, n_z, s_b, l_{\text{fus}}), \tag{10}$$

where $\chi_{\text{fus}}$ denotes the technology factor for the fuselage.

Additionally to the body surface, Prouty and Johnson take the fuselage length and the maximum take-off mass into account. Thus, they introduce a dependence on the geometric shape and overall weight. The inclusion of the maximum take-off mass can be seen as a first step towards an overall consideration of the rotorcraft: As mentioned earlier in Eqs. 3–5, $m_{\text{mto}}$ is partly the sum of the group masses which in turn are the sums of the corresponding component masses that are integrated into the helicopter. Depending on the intended operational use of the helicopter, certain mission equipment is not considered during the design, e.g., civil transport helicopters do not need ballistic protection, while avionics on military helicopters may include electronic countermeasures and identification friend or foe systems. Optical and infrared cameras, dunking sonar and search radars for anti-submarine helicopters will likely not be installed on civil helicopters. The installation of such systems may strongly influence the design gross weight, even when the geometric properties are the same for two different rotorcraft configurations.

Taking a closer look on the methods provided by Prouty (Eq. 11)

$$m_{\text{fus}} = 6.9 \cdot \left(\frac{m_{\text{mto}}}{1000}\right)^{0.49} \cdot l_{\text{fus}}^{0.61} \cdot s_b^{0.25}, \tag{11}$$

and Johnson

$$m_{\text{fus}} = \chi_{\text{fus}} \cdot 5.896 \cdot f_{\text{ramp}} \cdot \left(\frac{m_{\text{mto}}}{1000}\right)^{0.4908} \cdot n_z^{0.1323} \cdot s_b^{0.2544} \cdot l_{\text{fus}}^{0.61}, \tag{12}$$

one can see that Johnson's method for the fuselage mass is very similar to Prouty's (neglecting minor deviations for two exponents, namely $s_b$ and $m_{\text{mto}}/1000$), except that Johnson utilizes additional scaling factors. Besides the factor that accounts for a cargo ramp installation, Johnson considers the ultimate design flight load factor. With this approach Johnson considers the expected operational use of the helicopter, i.e., mission requirements, respectively, flight maneuvers which strongly influence the structural design. As an example, a Utility Transport Helicopter (UTH) of (approximately) the same (geometric) size and/or design gross weight can be expected to experience less severe maneuvers. In contrast, a combat helicopter is supposed to conduct more challenging maneuvers than the UTH, e.g., narrow turns or hard pitch downs. Therefore, the military helicopter is expected to experience higher load factors, so the structural demand is higher which in turn requires a stiffer airframe potentially resulting in a higher structural mass. Figure 14 shows a comparison of Prouty's and Johnson's method for the fuselage mass estimation as a function of the body surface $s_b$ and the fuselage length $l_{\text{fus}}$. It can be observed that Johnson's method (illustrated by the spectral color map) corresponds to the one provided by Prouty (illustrated as blue surface) with an offset which is caused by the additional scaling parameters. It is also observable, that a bigger helicopter (i.e., $s_b$ and/or $l_{\text{fus}}$ increase) entails a mass increase.

Table 3 shows the calculated fuselage masses applying Prouty's and Johnson's method to the aforementioned urban mobility concepts, assuming

$f_{\text{ramp}} = 1.0$,
$n_z = 3.5$, and
$\chi_{\text{fus}} = 1.0$,
for Johnson's method.

It can be seen, that the methods of Prouty and Johnson calculate a much lighter fuselage. Moreover, it can be

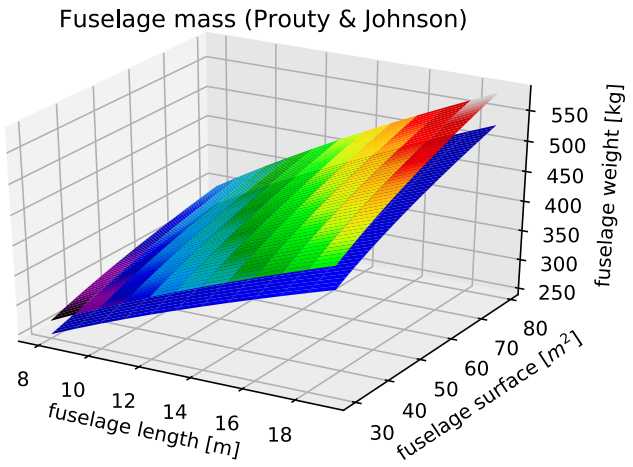


**Fig. 14** Fuselage mass calculation (Prouty and Johnson) as function of body surface and fuselage length

**Table 3** Estimated fuselage masses (Prouty and Johnson) for urban mobility concepts (values rounded)

| Rotorcraft | $m_{\text{mto}}$ [kg] | Prouty [kg] | Johnson [kg] |
|---|---|---|---|
| Volocopter | 450 | 49.33 | 48.70 |
| Volocopter ($f = 0.9$) | | 48.04 | 47.42 |
| Volocopter ($f = 0.8$) | | 46.65 | 46.02 |

observed that the application of surface correction factors do not severely influence the estimated mass, indicating a stable mass estimation. It shall be mentioned, that applying technology factors to account for advanced technologies, e.g., new materials, may further reduce the estimated weight. However, it shall be taken into account that all empirical models mentioned above were derived with respect to a fuselage comparable to the assembly shown in Fig. 5. A calibration of these models with a more sophisticated analysis performed in the preliminary design stage can minimize these uncertainties. The estimation of the component masses is not only important for the calculation of an updated $m_{\text{mto}}$ in the context of the conceptual sizing loop but also for the mass distribution for subsequent analysis with higher fidelity tools, e.g., in the preliminary design stage as described in Sect. 5.

## 5 Computational mass assessment

As already mentioned, the conceptual design approach to estimate the fuselage mass depends on statistics and gives only a rough estimate. It often does not take into account specific performance requirements like flight maneuvers, or specific configurations, such as high-speed compound configurations that usually feature additional thrust devices and, depending on the rotorcraft concept, lifting surfaces. Due to the continuously increasing computational power nowadays, a Finite Element (FE) analysis module was integrated into IRIS. This tool requires more input, quantitatively and qualitatively seen, than the conceptual design tools mentioned above. The computational time and the time required for the processing of input and output are also higher. Therefore, it is considered as L2 tool, representing preliminary design stage. Subsequently the model generation, the analysis, and an implemented sizing routine for static and quasi-static load cases will be introduced.

### 5.1 Model generation

At the end of the conceptual design stage the outer fuselage shape, i.e., the loft, has been determined. To continue with a structural FE analysis, the stiffness distribution must be known. Therefore, as a first step in the preliminary design phase, the primary structure is defined within the prescribed loft. Knowledge based design criteria are used to distribute skin reinforcements such as frames and stringers, e.g., cutouts must be reinforced. In addition, hard points that are used for the integration of key components, such as the rotors, gear box, and alighting gear, or other heavy components, must be attached to reinforced structure. Figure 15 shows the applied scheme (for visibility reasons the skin panels have been removed): The first step denotes the conceptual design phase, at the end of which an outer fuselage loft has been derived with the external configuration. Further requirements concerning cutouts and main frame positions have also been elaborated. Now—depending on the operational boundaries—the primary structure can be defined. The figure exemplary shows four different possible airframe configurations which are all based on the same rotorcraft loft. Each configuration will result in a different structural mass when analyzed, respectively, sized according to the expected ground- and flight load cases.

Currently ANSYS Parametric Design Language (APDL) is used for the model generation allowing parametric modeling and automated execution. The airframe is modeled using an approach as introduced by Hunter [31]: Stringers are discretized using elastic beam elements (BEAM188) that offer provision with arbitrary cross sections which allows the direct transfer of the profile data as described in the CPACS file. Applying the /ESHAPE command in ANSYS allows a visualization of the provided cross section(s). Frames are discretized as extruded profiles using elastic shell elements (SHELL181). Along

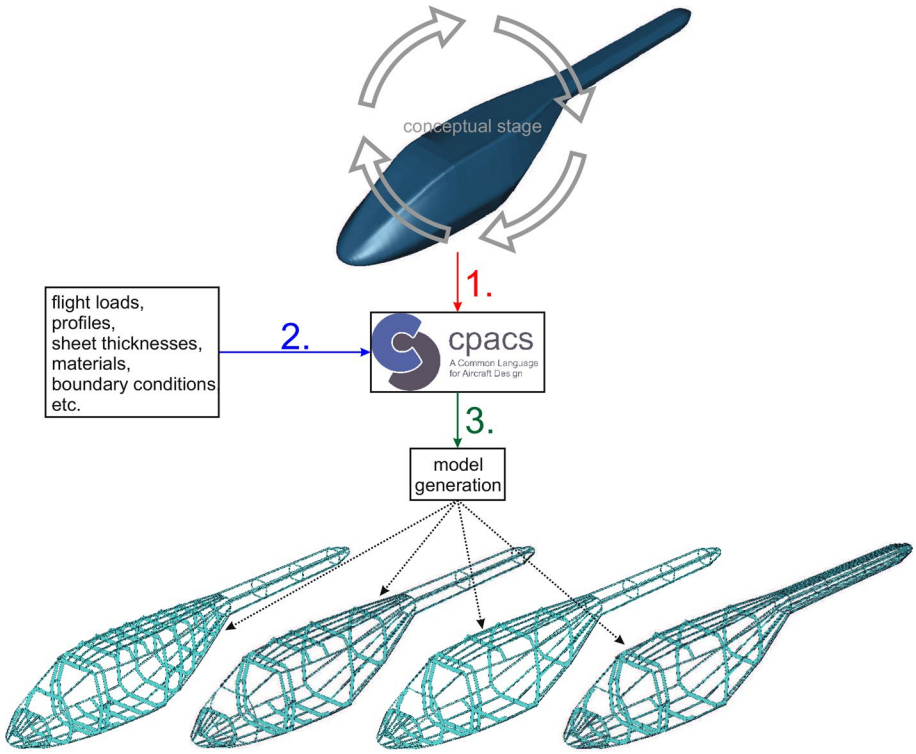


**Fig. 15** FE model preparation

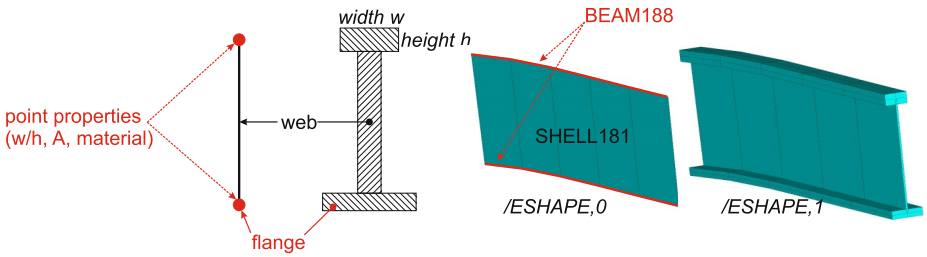


**Fig. 16** Mixed frame discretization

their edges beam elements (BEAM188) can be applied to account for any flanges, as shown in Fig. 16.

By default, the mesh is of Global Mesh Quality (GFEM) which means that each bay (that is defined by two adjacent stringers and frames) forms one shell element representing the skin panels. An algorithm analyzes the frames and stringers and calculates their intersections. At each intersection an interpolation point is generated that serves as node in the following model generation. Moreover, the GFEM approach does not feature joint element modeling, e.g., rivets or cleats that connect frames and stringers to each other as well as to the skin panels. This additional mass increase is taken into account with an additional mass factor, scaled to the fuselage mass. Shanley [32], for instance, numeralizes the mass increase due to joints in the range of 20–40% of the ideal minimum mass for metallic structures.

An FE model of a generic light utility helicopter airframe with cutouts for the windshield and doors is shown in Fig. 17.

So-called structural elements (consisting of profiles and material properties) are extruded either in longitudinal (stringers) or circumferential (frames) direction. Considering the stringers this approach would lead to an unreasonable stiffness and mass increase of the tail boom. Therefore, a virtual dummy structural element type none was implemented in the model generation. Dividing a structural member, i.e., stringer or frame, into several stages allows applying different structural elements to one structural member. This approach is called stage modeling and allows the provision with the virtual dummy element. This method is used to virtually reduce the stringers of the tail boom representing a realistic stiffness distribution and mass for the tail (see Fig. 18). Moreover, stage modeling is used to describe cutouts for passenger or cargo doors.

As indicated earlier do the interpolation points determine the airframe structure. The more interpolation points are available the better the fuselage loft can be represented. Therefore, virtual dummy elements can be used

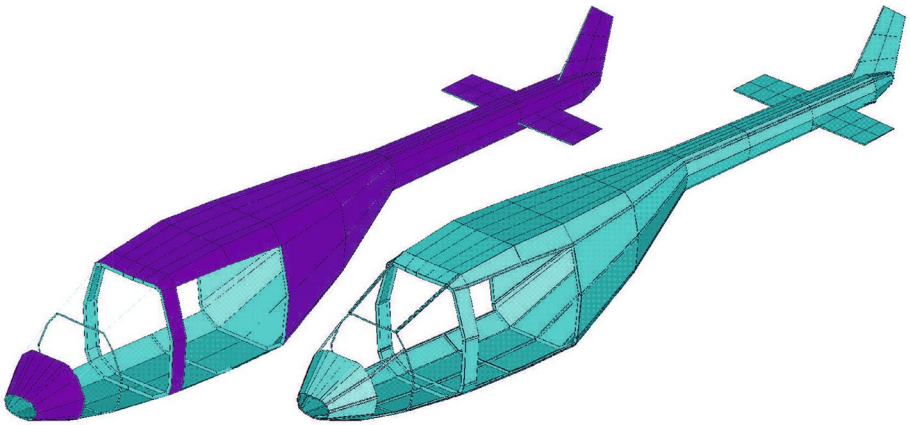

**Fig. 17** FE model (left side / ESHAPE,0 and right side / ESHAPE,1)

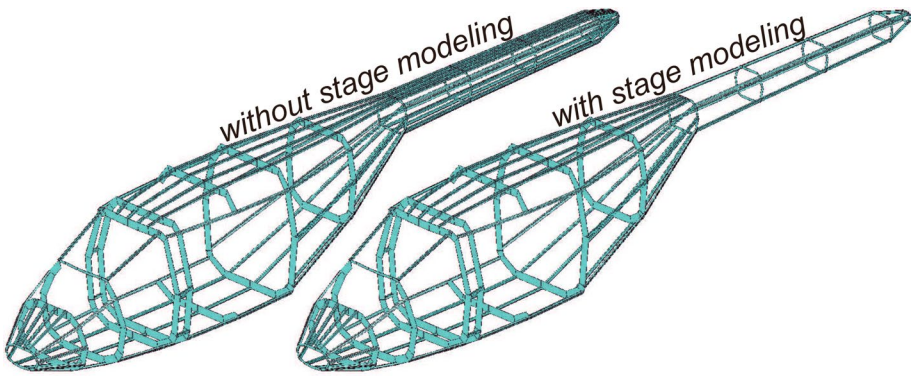


**Fig. 18** Stage modeling applied to the tail boom

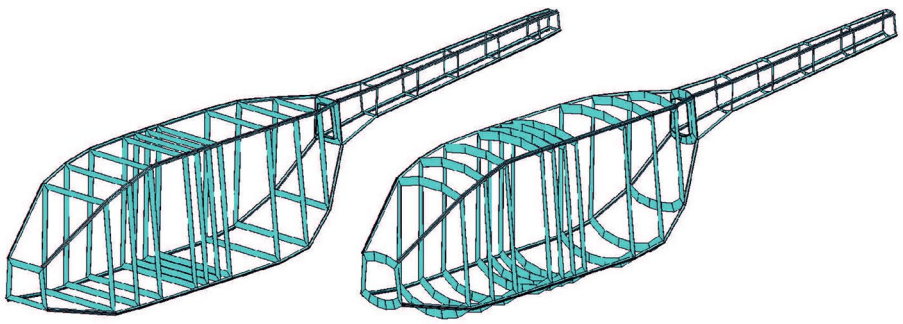

**Fig. 19** Influence of the amount of interpolation points on the model accuracy

to artificially increase the amount of interpolation points and, thus, to generate a geometrically more realistic airframe. Figure 19 shows an exemplary airframe with only four stringers. On the left a comparably coarse geometry is shown, while the model on the right shows the same airframe with additional stringers featuring the virtual dummy elements at the top and bottom side of the fuselage. Therefore, the model on the right features more interpolation points. It can be seen that this model features a smoother bottom and top surface representing the fuselage loft more precisely, while the model on the left strictly connects both lower and upper stringers, respectively, with straight elements.

More details on the modeling approach and on specific options, such as the structural element type none, cutouts, and stage modeling are given by Schwinn [33].

The component masses that have been estimated during the conceptual design phase are modeled as lumped masses at additional nodal points. They are constrained to the airframe over a user-specified region, as exemplary shown in Fig. 20.

External forces and moments generated at the rotors are applied at the corresponding nodes and constrained to a user-specified region of the airframe. Figure 20 exemplary shows the airframe (without skin panels for visibility reasons) and two nodal masses representing the main and tail rotor. At

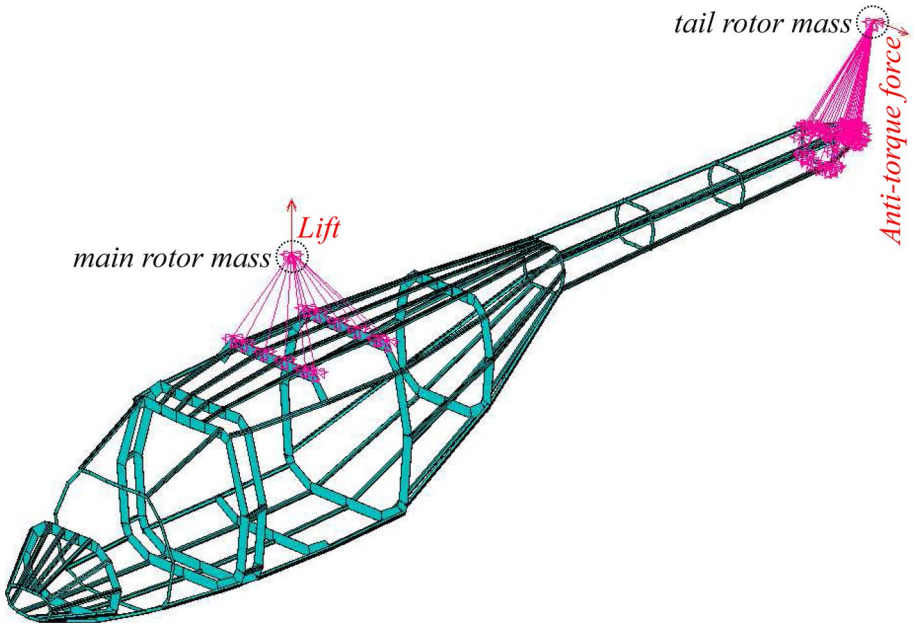


**Fig. 20** Force and mass constraints

each node the acting force is displayed by the red arrow, while the constraints that introduce the load into the airframe are shown in magenta. This modeling approach conditions that external forces (and moments) can only be applied at nodes representing nodal masses. Gravity is modeled as an acceleration field acting on all structural nodes and elements.

The model is fixed in space at a node close to the computed Center Of Gravity (COG). Potentially remaining forces due to little load inconsistencies during trim are compensated using the inertia relief option. This approach allows the calculation of stresses and strains without dynamic analyses by introducing artificial boundary conditions for equilibrium of forces and moments. The loads calculation uses the fuselage mass which has been estimated during the conceptual design phase for the calculation of the required lift forces. A more detailed description of the loads calculation process as it is currently implemented is given by Schwinn et al. [34]. To conclude the model generation section it shall be noted that currently only isotropic materials are implemented for the computational analysis. However, it is intended to integrate orthotropic materials into the analysis process during the TRIAD project. Depending on a user-specific entry in the CPACS file it is possible to either merely generate an FE model, to conduct a static analysis of a chosen load case (see Sect. 5.2), or to conduct a sizing process (see Sect. 5.3).

## 5.2 Static analysis

Static analyses are conducted using the linear-elastic solver in ANSYS. Exemplary, a hovering analysis of a generic utility rotorcraft with cutouts for the pilot doors (2x), cabin doors (2x) and for the windshield is shown in Fig. 21: The left figure displays the airframe, while—for visibility reasons—the skin panels have been removed in the center graph. The right graph shows the frames only. The fuselage structure is made of aluminum 2024 with flat frames of different heights. The thicknesses of the frames vary between $1.4 \leq t \leq 1.6$ [mm], while the skin panels feature a thickness of $t = 1.0$ [mm] and the hat shaped stringers feature sheet thicknesses of $t = 1.4$ [mm]. The material properties are displayed in Table 4.

It can be observed from Fig. 21 that the highest stresses arise, where the heaviest masses are located and the external loads from the rotors are introduced. It can also be seen that due to the fuselage cutouts the load is transferred around the cutout in the adjacent frames, while the highest stress is located in the center frame of the cutout, where the main rotor is located. Additionally, it can be observed that the lateral force generated by the tail rotor (to compensate the torque of the main rotor) leads to a stress increase at the transition frame between fuselage cabin and tail boom. The tail boom can be considered as a beam under bending load clamped at the aforementioned transition frame.

**Table 4** Aluminum 2024 - material properties

| Parameter | Value |
|---|---|
| Young's modulus [GPa] | 67.7 |
| Density $\rho$ [kg/m$^3$] | 2800 |
| Poisson's ratio [−] | 0.248 |
| Yield strength [MPa] | 320 |

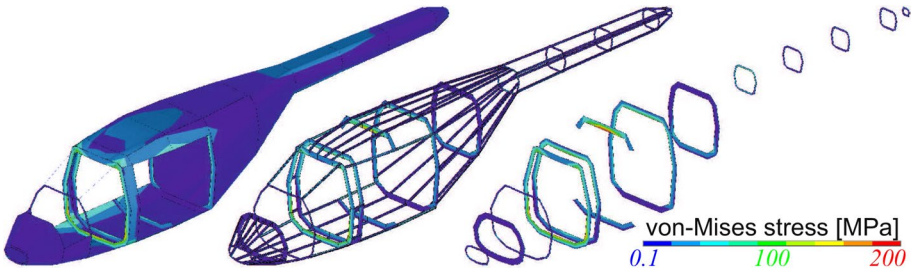


**Fig. 21** Static hovering analysis (coarse discretization)

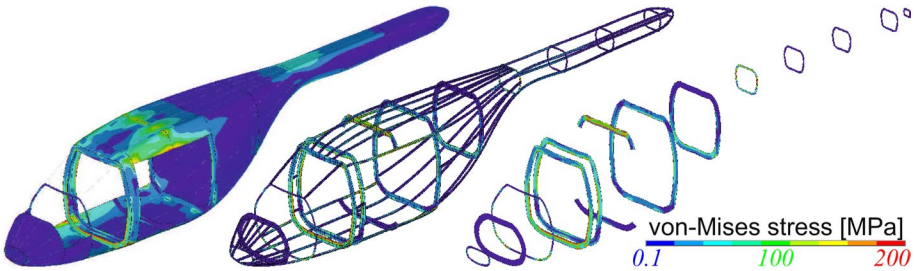


**Fig. 22** Static hovering analysis (fine discretization)

Applying a finer discretization in Detailed FEM (DFEM) quality to the same model, as shown in Fig. 22, a mesh dependent behavior can be observed.

This dependence is substantiated that the mesh is not fine enough to calculate local stress peaks, so the stresses are averaged over the larger areas, i.e., the larger element sizes. Therefore, localized stress concentrations cannot be adequately shown with the coarse GFEM approach. However, it shall be noted that for preliminary purposes, the GFEM approach is considered as sufficient because of the faster pre- and post-processing, faster computations, and smaller file sizes in relation to the required level of detail.

### 5.3 Sizing approach

Structural sizing is conducted using an APDL based sizing module. It was originally developed for sizing of aircraft wings [35] and enhanced to size transport aircraft fuselages [36]. During the EDEN project it was extended for the use of rotorcraft fuselages [37]. Sizing is based on Fully Stressed Design (FSD) principles. Strength evaluation is conducted using the equivalent stress. To guarantee sufficient safety against stability failure, local compressive and shear buckling methods as provided by Bruhn [38] and Niu [39] have been implemented.

For each element the equivalent stress $\sigma_{\text{eqv}}$ is computed. The safety factor against strength failure $SF_{\text{str}}$ is calculated as

$$\text{SF}_{\text{str}} = \frac{\sigma_{\text{eqv,max},a}}{\sigma_{\text{eqv}}}, \tag{13}$$

where $\sigma_{\text{eqv,max},a}$ describes the maximum allowable equivalent stress, as specified by the material limits (in the CPACS file). It shall be noted that safety factors can be specified in the CPACS file to adjust the material limits.

Additionally, each element is investigated for stability. Buckling under combined loading (compression and shear) is evaluated using the ratios

$$R_c = \frac{\sigma_c}{\sigma_{c,\text{crit}}}, \tag{14a}$$

and

$$R_s = \frac{\tau}{\tau_{\text{crit}}}, \tag{14b}$$

so that the safety factor against instability $\text{SF}_{\text{stab}}$ can be calculated as the ratio of the critical to the actual stress condition (as shown in Fig. 23):

$$\text{SF}_{\text{stab}} = \frac{\overline{\text{OB}}}{\overline{\text{OA}}} \tag{15}$$

In Eq. 15, O denotes the origin and $A(R_{\text{sA}}|R_{\text{cA}})$ describes the actual stress condition. The point $B(R_{\text{sB}}|R_{\text{cB}})$ marks the begin of buckling (Fig. 23). It is an extension of the line $\overline{\text{OA}}$ that intersects the failure curve which is described as

$$R_s^2 + R_c = 1. \tag{16}$$

The most critical safety factor is then used to scale the thickness of each element. Shell elements are sized by their sheet thickness, while all sheet thicknesses of beam elements

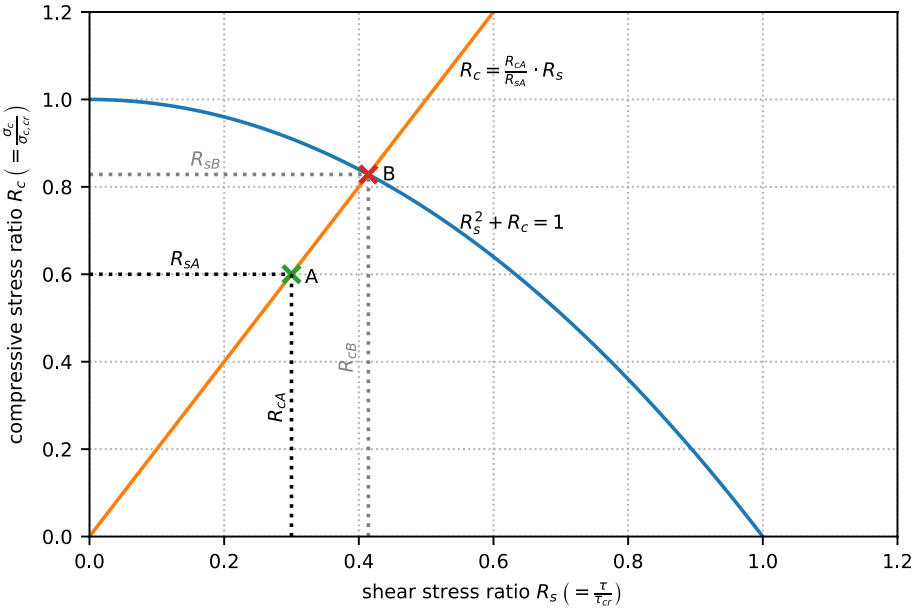


**Fig. 23** Compressive and shear buckling interaction

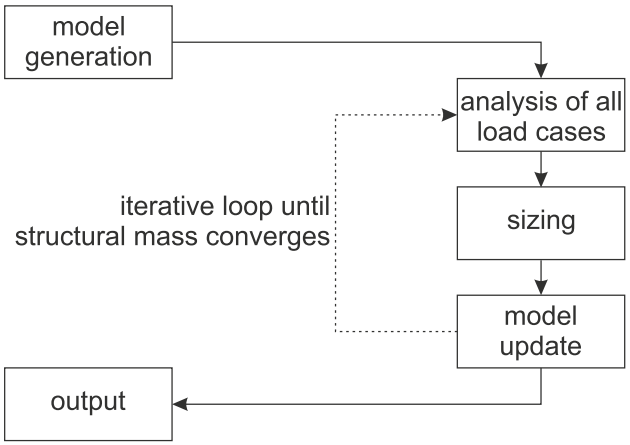


**Fig. 24** Flowchart of the structural sizing module

are scaled equally maintaining its basic cross section, as exemplary shown in Fig. 31.

This process is repeated for each specified load case and the maximum required element thickness, respectively, sheet thicknesses are stored. The stress states in all elements are then recalculated with the updated stiffness distribution until convergence is achieved, as schematically illustrated in Fig. 24. The final thicknesses and cross sections are saved in the CPACS file as well as the updated mass breakdown due to the new values for $m_{\text{struct}}$, $m_{\text{oem}}$, and $m_{\text{mto}}$.

This step allows feedback to the conceptual design loop to allow a resizing of the external configuration with respect to special performance requirements affecting the structural design. An exemplary sizing process for a light utility helicopter, as illustrated in Fig. 20–22, is displayed

**Table 5** Load case description

| Model number | Load case (added) |
|---|---|
| 01 | Hovering |
| 02 | 01 + maximum cruise |
| 03 | 02 + jump take-off |
| 04 | 03 + turns |
| 05 | 04 + 2.5g pull |

in Fig. 25. The load cases that were used for the sizing are listed below in Table 5.

Figure 25 shows the mass development (logarithmic) over iterations with increasing number of considered load cases converging in general after five to six iterations. It can be seen, that the mass increases due to the addition of new load cases with the 2.5 g pull maneuver evoking the highest mass. However, it must be noted that the sole calculation of the 2.5 g pull cannot be seen sufficient for the structural sizing, since several load cases call responsible for different areas of the airframe.

Model 06 corresponds to model 05, except that the finer discretization approach has been chosen (see Table 6).

The weight estimated using the calibrated AFDD models is represented by the dashed line. The red marker in the converged iteration number six (It-06) with the error bars represents the additional weight range of the joints (applied to model 05) as proposed by Shanley indicating good agreement of the statistical and the numerical approach at this early design stage. The stringer sizing allowed a wide range, potentially scaling the sheet thicknesses $t$ of each stringer Si in a range of

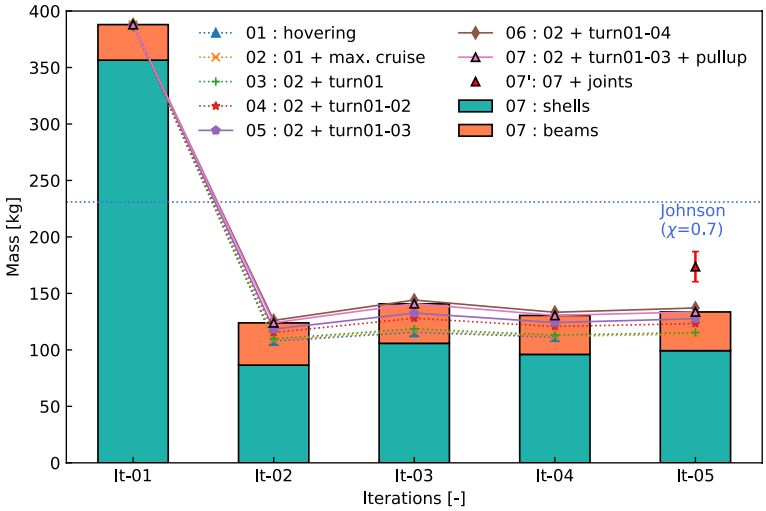


**Fig. 25** Sizing process for an UTH

**Table 6** Discretization approaches (rounded values)

| Model | Nodes | Shells | Beams | Time [s] |
|---|---|---|---|---|
| 05 (coarse) | 650 | 480 | 100 | 156 |
| 06 (fine) | 8830 | 7250 | 960 | 638 |

$$0.5 \cdot t_{(\mathrm{Si,original})} \leq t_{(\mathrm{Si,new})} \leq 5.0 \cdot t_{(\mathrm{Si,original})}. \quad (17)$$

Comparing model 05 and model 06 to each other it can be noted that the finer discretization results in a slightly higher mass—caused by the increased amount of nodes and elements that represent the geometry more accurate compared to the coarse model. However, it must be noted that the increase in computational time to conduct the sizing process may—depending on the available resources—exceed the acceptable time regarding preliminary design level with regard to a possible global resizing with L1 tools.

Figures 26 and 27 show the resulting thickness distribution for the shell elements (representing the frames and the skin panels) for the coarse and fine discretization. As seen at the static computation, the stresses in the coarse computation are averaged over a larger area so that the required thicknesses are comparably less. In contrast, the finer discretization shows higher required local thicknesses for some critical areas, such as the frame between the cut-outs for the doors or the frame, where the main rotor is attached to.

As mentioned above, the airframe is sized due to the influence of different load cases at different areas. Figure 28 overviews the airframe and its dependence on the specified load case. The numbers that are specified in the legend refer to the number depicting the individual load case as given in Table 5 and Fig. 25 (with 3a and 3b representing different turns).

Figure 29 shows the relevant sizing criteria for the shell elements. It can be observed that most of the elements are sized either according to strength limits (maximum von Mises stress), shell buckling criteria, and the minimum thickness criteria. The minimum thickness criterion is applied, since the surrounding stringers take a significant share of the load.

Figure 30 visualizes the stringer sizing using different colors. The original model before sizing had an identical stringer distribution, i.e., all stringers had the same cross section and material properties.

Section 1 (S1) represents the original stringer profile, as depicted by the hatched profile in Fig. 31.

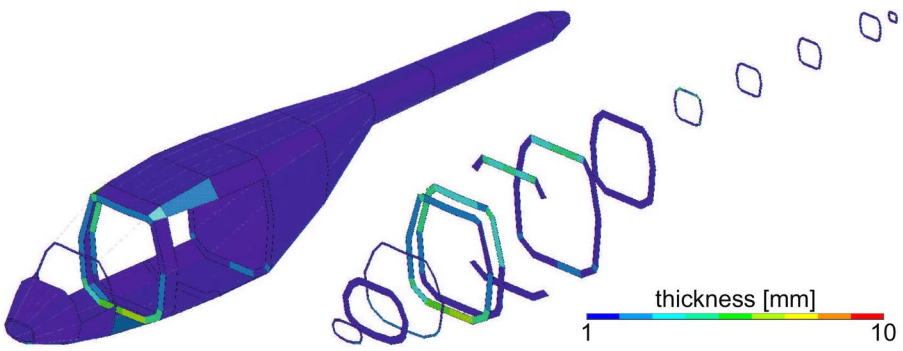


**Fig. 26** Model 05: Thickness distribution

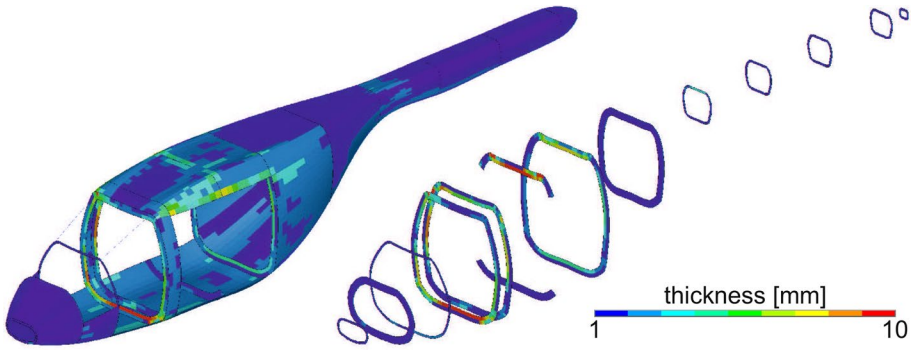


**Fig. 27** Model 06: Thickness distribution

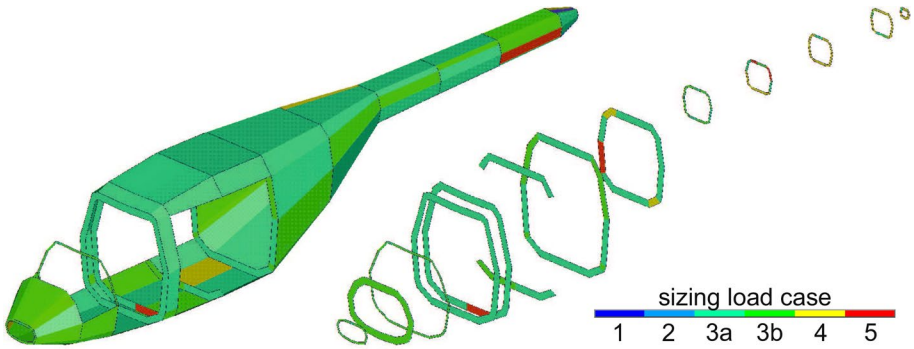


**Fig. 28** Model 05: Critical load cases

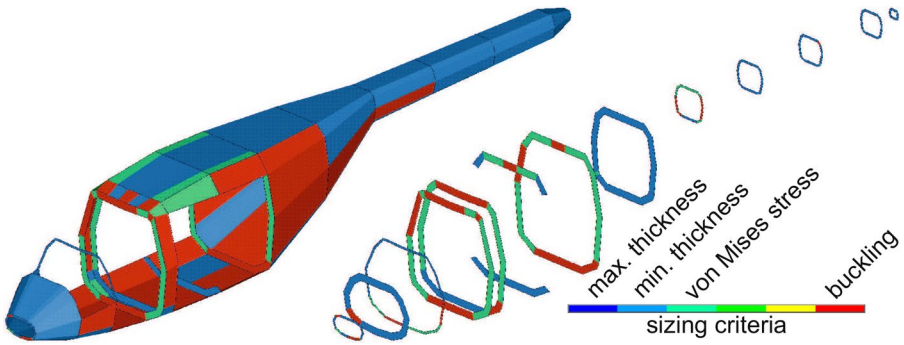


**Fig. 29** Model 05: Sizing criteria

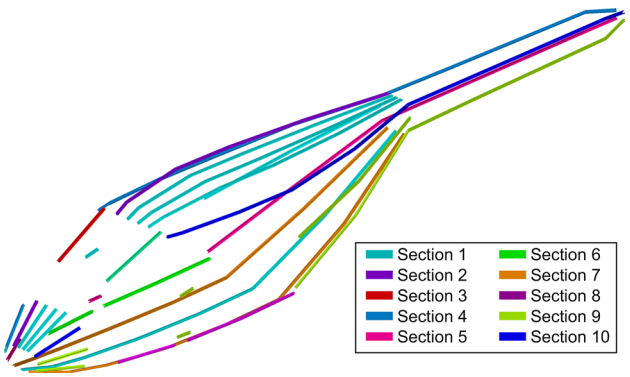


**Fig. 30** Model 05: Stringer sizing

Exemplary, section 2 (S2) is illustrated in red in Fig. 31. As mentioned above, beam elements are sized by equally scaling their sheet thicknesses. The sheet thicknesses of section 2 correspond to

$$t_{S2} = 2.2 \cdot t_{S1}. \tag{18}$$

It can be seen that section 2 shows similar but scaled sheet thicknesses compared to the shape of the original omega-hat-shaped geometry S1 (Table 7).

## 6 Discussion of the results

The presented process chain to evaluate rotorcraft masses during early design stages consists of two consecutive phases. Hence, there are two different levels of detail.

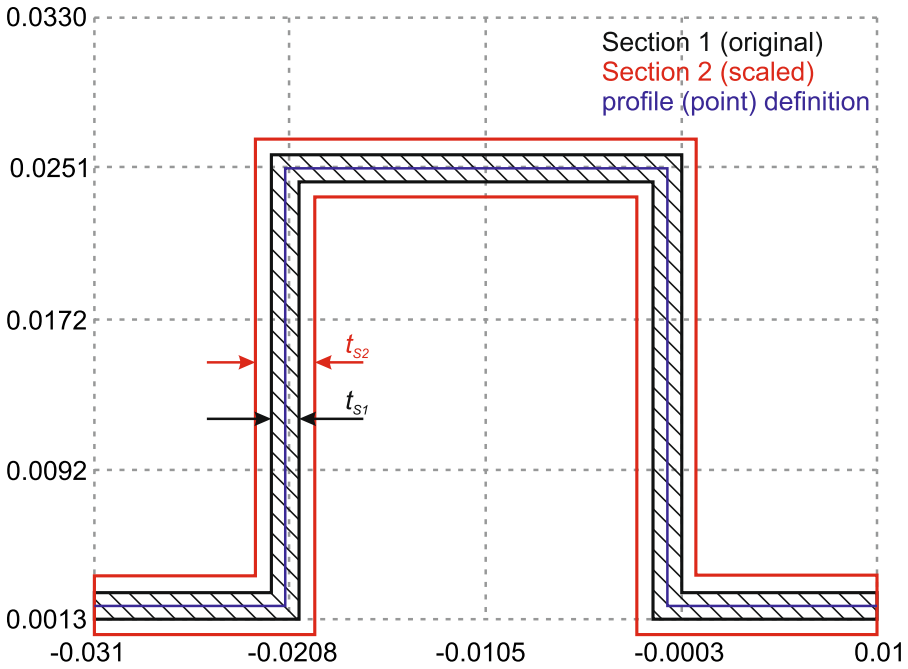


**Fig. 31** Sizing of stringer sections

**Table 7** Stringer section properties

| Parameter | Section 1 | Section 2 |
|---|---|---|
| Area | 0.122*E*–03 | 0.268*E*–03 |
| $I_{yy}$ | 0.105*E*–07 | 0.234*E*–07 |
| $I_{yz}$ | -0.326*E*–09 | –0.718*E*–09 |
| $I_{zz}$ | 0.145*E*–07 | 0.320*E*–07 |
| Warping constant | 0.704*E*–12 | 0.167*E*–11 |
| Torsion constant | 0.940*E*–10 | 0.999*E*–09 |
| Centroid Y | –0.010764 | –0.010764 |
| Centroid Z | 0.013368 | 0.013368 |
| Shear Center Y | –0.011267 | –0.011258 |
| Shear Center Z | 0.033024 | 0.032895 |
| Shear Correction YY | 0.222209 | 0.225351 |
| Shear Correction YZ | –0.003756 | –0.00362 |
| Shear Correction ZZ | 0.581874 | 0.595518 |

During the conceptual design phase statistical models are used to estimate the overall rotorcraft mass for subsequent flight performance analyses. Several methods were applied for a generic UTH based on an enhanced EC135 (Fig. 7). The estimated masses showed major deviations to each other for some components but, if summed up to superordinate masses, e.g., $m_{\mathrm{mto}}$, close results. For the presented generic UTH, an overall technology factor of $\chi = 0.7$ was applied for Johnson's methods and showed very good results compared to the reference mass. As mentioned before, an overall technology factor might be debatable, because errors, respectively, deviations for individual components may cancel each other but can be accepted for mass estimation during the conceptual design before detailed knowledge during the proceeding design process is gained.

The same technology factor was applied for a mass estimation of a Bo105 (Fig. 8), which corresponds to a rotorcraft of a similar configuration. Comparing the results for both rotorcraft, $\chi = 0.7$ seems to be an acceptable overall technology factor for this weight class.

It could be shown that the mass estimation methods of Beltramo and Morris, and also Layton showed a larger deviation to the reference mass. This circumstance is caused by the comparably small amount of parameters to describe the rotorcraft system. The methods by Palasis, Prouty, and Johnson yielded results that were close to the reference mass but also to each other. Their deviation to the reference mass was less than 5% which is within acceptable bounds for the conceptual design stage. The methods by Palasis are a mixture of the methods provided by Beltramo and Morris, and Layton. However, his mixture of both approaches leads to decent results with only a small amount of parameters that have to be designed in advance, thus appearing ideal for a fast mass estimation at early design stages. However, it must be explicitly mentioned that the methods in this paper were only applied to rotorcraft of medium size class. The methods of Prouty and Johnson require much more parameters, thus allowing a very precise mass estimation of individual components. As disadvantage, these parameters must either be estimated wisely or be calculated which requires the integration of many other disciplines.

For novel, unusual designs (in the context of classic rotorcraft configurations), such as air taxis, it could be shown

that the older methods by Beltramo and Morris, and Layton can lead to negative masses. Those rotorcraft configurations should be estimated using the methods by Prouty or Johnson. For these types, the large amount of parameters allow a more detailed mass estimation, because they are based on newer rotorcraft with advanced technologies, such as the extensive use of composite materials in recent years.

For a mass calculation at preliminary design phases, an automated FE tool was integrated in the design process, based on a parametric model description. An exemplary sizing process with some selected load cases was conducted at GFEM detail level and the results presented in detail. The highest airframe loads occurred at the frames close to the load introduction of the main rotor, respectively, main gear box and at the reinforcements of the door cutouts leading to the highest thicknesses (Fig. 26). The presented sizing process with a limited amount of flight- and ground load cases showed a lower fuselage mass than estimated with statistical methods (Table 5), caused by the comparably low detail level (Fig. 25), e.g., GFEM models do not include joint elements. Joints were estimated with an additional mass increase of 30% of the undisturbed fuselage structure, as proposed by Shanley. But even with the addition of this joint elements mass, the FE computation shows a lower fuselage mass because of the detail level. Additional masses, such as windshield, doors, and their opening and locking mechanisms are missing in the FE model. Every cutout of the undisturbed fuselage implies a higher mass increase than the pure lack of the cut fuselage skin. Moreover, a vibration analysis is not (yet) included in the sizing process which often requires additional masses to dampen the structure. Therefore, the results of the presented FE sizing process should not be seen as a quantitative replacement of the mass estimation with statistical methods. However, it can be seen as a first step towards an assessment of the fuselage mass with mission dependent characteristics which allows an individual, more detailed mass analysis of (especially) novel rotorcraft configurations.

The comparison between a fine and a coarse FE discretization showed comparable results with higher computational expenditure for the fine approach. A finer discretization of the fuselage led to a higher mass due to a more accurate geometrical representation of the structure. Increasing numerical power will allow the application of the fine discretization for future sizing analyses. However, it shall be noted at this point that, to account for manufacturing aspects (for instance, one common thickness for the complete panel), individual elements of the fine discretization must be grouped together into optimization regions corresponding to the panels as they are manufactured, i.e., the thickness of the critical element determines the thickness of the complete panel.

Concluding the FE approach it shall be mentioned that a mass increase during the design is a common circumstance. Even after the detailed design phase, mass increase is not unusual—not only between the detailed design phase and the first flight (about 5–15%) but also afterwards (up to about 5%), as shown by Raymer [40]. He states as sources of weight growth, i.a., overspecification of requirements, addition of features and capabilities, incorrect loads estimation, excessive safety, poorly-understood advanced technologies, problem fixing (e.g., stability, flutter, fatigue, propulsion, etc.), materials and components selection. Therefore, a quantitative determination of a common general factor that might be used to scale the airframe mass of the preliminary design stage to compare it to masses estimated with statistical methods, seems inadequate and must be treated carefully: in that case, a design draft would be compared to a rotorcraft that is already in operational use, i.e., it has already undergone all the mass changes after the design had been frozen.

## 7 Conclusion and outlook

The presented paper introduced the design environment IRIS with particular focus on the mass assessment. The highly modular approach of the process chain combined with the use of CPACS as data model allows a flexible arrangement of the tools. This is, in particular, important, because the presented process chain is under steady development, for instance the extension on hybrid, respectively, battery powered rotorcraft. These types feature fundamental differences to the classic configurations, e.g., the lack of a fuel system or gear boxes and the integration of batteries and electric engines.

Methods to estimate the mass breakdown of a rotorcraft configuration were presented for the conceptual design and preliminary design stages. The approaches to estimate the fuselage mass were explained in detail and their ad- and disadvantages were highlighted.

To profit at early design stages from the steadily increasing numerical power, an approach to numerically size the fuselage to calculate its structural mass was introduced. Exemplary analyses and sizing processes were shown.

To further enhance the presented mass estimation methods, future enhancements comprise:

- The integration of composite materials will allow tailoring of the material according to the load paths, thus promising significant weight saving potential.
- To reduce the dependence on commercial FE solvers and, therefore, license availability and costs, the presented FE module will be reconstructed and integrated into the solver independent framework software PANDORA

(Parametric Numerical Design and Optimization Routines for Aircraft, [41]) which is currently under development at the DLR Institute of Structures and Design.
- The loads calculation process will be transferred to HOST to integrate more flight maneuvers and, therefore, load cases into the sizing process. Moreover, it is intended to extend the loads analysis by integration of gust and vibratory loads, because rotorcraft are exposed to a high level of vibrations which are usually dampened out by placing additional masses.
- A more detailed, and therefore, more realistic mass distribution that dispenses with nodal point masses, is required to improve the static analysis and sizing routines. Moreover, a more detailed mass distribution may allow an extension of the considered load cases and also additional dynamic assessment of the fuselage. The more detailed mass distribution, in turn, calls for the use of finer discretized models. It is expected that the continuously increasing numerical power will reduce the higher times required for model generation and sizing, thus allowing the application for DFEM models in the presented process chain.

**Acknowledgements** The work presented in this manuscript has been achieved within the DLR projects EDEN, FAST-Rescue (Fast and Silent Rescue Helicopter), and TRIAD. The authors would like to gratefully acknowledge and appreciate the financial support. Additionally, the authors would like to express their gratitude to Dieter Kohlgrüber, Joachim Götz, Jonas Jepsen, Arthur Zamfir, Thomas Weber, and Christian Haschert for their valuable contribution to TRIAD and the fruitful discussions.

**Conflict of interest** The authors declare that they have no conflict of interest.



## References

1. Raymer, D.: Aircraft design: a conceptual approach, 2nd edn. AIAA, Washington (1992)
2. Lier, M., Harbig, K., Kohlgrüber, D., Krenik, A., Kunze, P., Lützenburger, M.: Studies on rotorcraft integrated design and evaluation at DLR—first results. In: Proceedings of the 38th European Rotorcraft Forum. Amsterdam, Netherlands (2012)
3. Lier, M., Kohlgrüber, D., Krenik, A., Kunze, P., Lützenburger, M., Schwinn, D.B.: Rotorcraft pre-design activities at DLR—results, status and outlook. In: Proceedings of the 40th European Rotorcraft Forum. Southampton, UK (2014)
4. Lier, M., Krenik, A., Kunze, P., Kohlgrüber, D., Lützenburger, M., Schwinn, D.B.: A toolbox for rotorcraft preliminary design. In: Proceedings of the 71st Annual Forum of the American Helicopter Society. Virginia Beach, VA, USA (2015)
5. Nagel, B., Böhnke, D., Gollnick, V., Schmollgruber, P., Rizzi, A., La Rocca, G., Alonso, J.J.: Communication in aircraft design: Can we establish a common language? In: Proceedings of the 28th International Congress of the Aeronautical Sciences (ICAS). Brisbane, Australia (2012)
6. Seider, D., Litz, M., Schreiber, A., Gerndt, A.: Open source software framework for applications in aeronautics and space. In: Proceedings of the 2012 IEEE Aerospace Conference. Big Sky, MT, USA (2012)
7. Weiand, P., Buchwald, M., Schwinn, D.: Process development for integrated and distributed rotorcraft design. Aerospace **6**(2), 23 (2019). https://doi.org/10.3390/aerospace6020023
8. Liersch, C., Hepperle, M.: A distributed toolbox for multidisciplinary preliminary aircraft design. CEAS Aeronautical J. **2**, 57–68 (2011). https://doi.org/10.1007/s13272-011-0024-6
9. homepage: TIXI. https://github.com/DLR-SC/tixi. Accessed on 22 Jan 2020
10. homepage: TIGL. https://github.com/DLR-SC/tigl. Accessed on 22 Jan 2020
11. Weiand, P., Schwinn, D., Schmid, M., Buchwald, M.: A multidisciplinary process for integrated rotorcraft design. In: Proceedings of the 43rd European Rotorcraft Forum. Milan, Italy (2017)
12. Krenik, A., Weiand, P.: Aspects on conceptual and preliminary helicopter design. In: Proceedings of the German Aerospace Congress (DLRK). Braunschweig, Germany (2016)
13. Kunze, P.: Parametric fuselage geometry generation and aerodynamic performance prediction in preliminary rotorcraft design. In: Proceedings of the 39th European Rotorcraft Forum. Moscow, Russia (2013)
14. Maskew, B.: Program VSAERO theory document: a computer program for calculating nonlinear aerodynamic characteristics of arbitrary configurations. Tech. rep., NASA, NASA-CR-4023 (1987)
15. Keys, C.N., Wiesner, R.: Guidelines for reducing helicopter parasite drag. J. Am. Helicopter Soc. **20**(1), 31–40 (1975). https://doi.org/10.4050/JAHS.20.31
16. Stepniewski, W.Z., Keys, C.N.: Rotary-wing aerodynamics–volume II: performance prediction of helicopters. Dover Publications Inc., Mineola (1984)
17. Benoit, B., Dequin, A.M., Kampa, K., von Grünhagen, W., Basset, P.M., Gimonet, B.: HOST, a general helicopter simulation tool for Germany and France. In: Proceedings of the 56th Annual Forum of the American Helicopter Society. Virginia Beach, VA, USA (2000)
18. Buchwald, M., Weiand, P., Schwinn, D.B., Schmid, M.: Flight performance calculation of rotorcraft in the conceptual design phase. In: Proceedings of the German Aerospace Congress (DLRK). Friedrichshafen, Germany (2018)
19. Weiand, P., Schmid, M., Buchwald, M., Schwinn, D.: A distributed design environment for rotorcraft. In: Proceedings of the German Aerospace Congress (DLRK). Friedrichshafen, Germany (2018)
20. Torenbeek, E.: Advanced aircraft design. Wiley, Chichester (2013)

21. Society of Allied Weight Engineers: SAWE RP No. 8A—weight and balance data reporting forms for aircraft (including rotorcraft and air-breathing unmanned aerial vehicles)—revision 1 (1997)
22. Beltramo, M.N., Morris, M.A.: Parametric study of helicopter aircraft systems costs and weights. Tech. rep., NASA, NASA-CR-152315 (1980)
23. Layton, D.M.: Introduction to helicopter conceptual design (1992)
24. Palasis, D.: Erstellung eines Vorentwurfsverfahrens für Hubschrauber mit einer Erweiterung für das Kipprotorflugzeug. Phd thesis, Universität der Bundeswehr, München (1992)
25. Prouty, R.W.: Helicopter performance, stability, and control. Krieger Publishing Company, Malabar (2002)
26. Johnson, W.: NDARC - NASA design and analysis of rotorcraft. Tech. rep., NASA, NASA/TP-2009-215402 (2009)
27. Kaletka, J., Kurscheid, H., Butter, U.: FHS, the new research helicopter: ready for service. Aerosp. Sci. Technol. **9**(5), 456–467 (2005). https://doi.org/10.1016/j.ast.2005.02.003
28. Russell, C., Basset, P.M.: Conceptual design of environmentally friendly rotorcraft—a comparison of NASA and ONERA approaches. In: Proceedings of the 71st Annual Forum of the American Helicopter Society. Virginia Beach, VA, USA (2015)
29. homepage: Volocopter. https://www.volocopter.com/de/product/. Accessed on 26 Jul 2018
30. homepage: Ehang 184 - specs. http://www.ehang.com/ehang184/specs/. Accessed on 1 Aug 2018
31. Hunter, E.W.: A process to enable high fidelity airframe sizing and optimization for conceptual design. In: Proceedings of the 49th AIAA/ASME/ASCE/AHS/ASC Structures, Structural Dynamics, and Materials Conference. Schaumburg, IL, USA (2008)
32. Shanley, F.: Weight-strength analysis of aircraft structures, 2nd edn. Dover Publications Inc, New York (1960)
33. Schwinn, D.B.: Applied parametrized and automated airframe modeling methods in the preliminary design phase. Int. J. Model. Simul. Sci. Comput. **6**(4), 1550037 (2015). https://doi.org/10.1142/S1793962315500373
34. Schwinn, D.B., Weiand, P., Schmid, M., Buchwald, M.: Structural sizing of a rotorcraft fuselage using an integrated design approach. In: Proceedings of the 31st Congress of the International Council of the Aeronautical Sciences (ICAS). Belo Horizonte, MG, Brazil (2018)
35. Nagel, B., Kintscher, M., Streit, T.: Active and passive structural measures for aeroelastic winglet design. In: Proceedings of the 26th International Congress of the Aeronautical Sciences (ICAS). Anchorage, AK, USA (2008)
36. Scherer, J., Kohlgrüber, D., Dorbath, F., Sorour, M.: A finite element based tool chain for structural sizing of transport aircraft in preliminary aircraft design. In: Proceedings of the German Aerospace Congress (DLRK). Stuttgart, Germany (2013)
37. Schwinn, D.B., Weiand, P., Schmid, M.: Structural analysis of a rotorcraft fuselage in a multidisciplinary environment. In: Proceedings of the NAFEMS World Congress. Stockholm, Sweden (2017)
38. Bruhn, E.F.: Analysis and design of flight vehicle structures. Tri-State Offset Company, Cincinnati (1973)
39. Niu, M.C.Y.: Airframe stress analysis and sizing, 2nd edn. Hong Kong Conmilit Press Ltd., Hong Kong (1999)
40. Raymer, D.P.: Why weights engineering is so dang important, and why weights engineers get all the blame. In: SAWE's Virtual Tech Fair for Mass Properties Engineers. SAWE (2020). Keynote Presentation
41. Petsch, M., Kohlgrüber, D., Walther, J.N.: Development of a fully automated transport aircraft fuselage modelling and sizing tool using Python. In: Proceedings of the German Aerospace Congress (DLRK). Munich, Germany (2017)